ABSTRACT

Wildland-urban interface areas are growing rapidly. Building standards are required to ensure that the structures built in fire prone areas are resilient to fire. Australian Standard AS 3959 was developed to prescribe construction requirements for houses in bushfire prone areas. The model in AS 3959 is applied to estimate the Bushfire Attack Level (BAL) that is expected on a structure during the nominally worst-case bushfire scenario that the house can experience. Once the BAL is based on the fuel and terrain near the structure, and determines the construction requirements for the structure. AS 3959 is based upon a view-factor model of radiant heat flux, which estimates the level of heat flux expected at the structure.

Peer-reviewed article

Simulations of radiation heat flux on a structure from a fire in an idealised shrubland

Khalid AM Moinuddin and Duncan Sutherland

1. Institute for Sustainable Industries and Liveable Cities, Victoria University.
2. School of Science, University of New South Wales.
3. Bushfire and Natural Hazards CRC.

The view-factor model essentially estimates how much of the fire is 'seen' by the structure. The example simulation shown in Figure 1 has a schematic of the view-factor model superimposed upon it. AS 3959 assumes (among other idealisations) a straight-line fire of 100 m width with a constant flame temperature of 1090 K, and seeks to maximize the view factor by varying the flame angle. In reality, flame temperatures can exceed 1200 K (Worden et al. 1997) and the flame angle is determined by the interaction of the buoyant fire plume and the driving background wind. Flame temperature is a critical parameter because it is raised to the fourth power in the model. As an illustrative example, if the flame temperature reaches 1400 K then the expected radiative heat flux will be approximately 175 % of the value if flame temperature was 1090 K. Flame angle varies greatly depending on whether a fire is dominated by buoyancy, or by the background wind and fires can transition between the buoyancy dominated and wind dominated modes.

Wind dominated fires have long, elongated flames that are close to the ground, whereas buoyancy dominated fires have tall, vertical plume-like flames. Obviously, the flame of a buoyancy dominated fire will have a larger view-factor than a wind dominated fire. However, wind dominated fires occur when the wind speed is high (for all other conditions equal). Because AS 3959 is based on empirical models which do not account for the differences between buoyancy dominated and wind dominated fires, AS 3959 could ignore a fire that gives higher radiative heat flux at lower driving wind speed. That is, the model in AS 3959 may not correctly predict what set of weather and fuel conditions give the worst-case scenario. AS 3959 is also considerably restricted by a lack of a model for ember attack. While the AS 3959 standard prescribes numerous requirements to mitigate against the risk of embers, there is minimal guidance about what ember risk is expected for given fire conditions.

Khan et al. (2019) simulated grassfires impacting on a structure and compared the simulated heat flux with the predictions of AS 3959. AS 3959 was found to somewhat under predict the heat fluxes in the higher BAL classifications. The fires simulated in Khan et al. were 20 m in width, and the radiative heat flux received at the structure was comparable with the BAL levels expected from a 100 m wide fire.

The width restriction in the simulations was due to computational time constraints, however, the results imply that the heat flux from a 100 m wide fire will likely

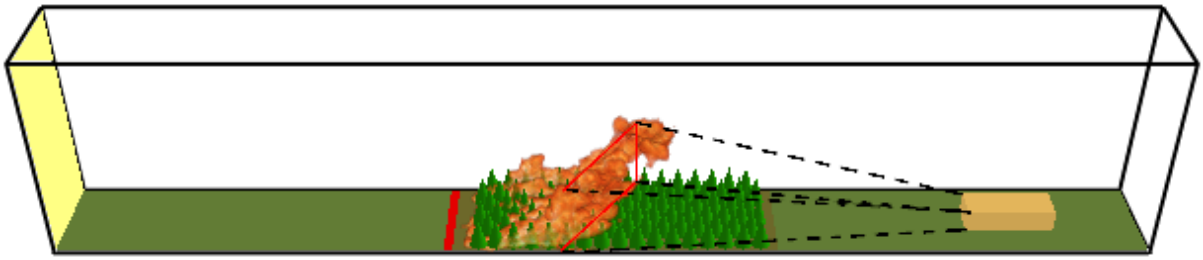

Figure 1: Rendering of the domain, with the fire at 34 s from ignition. The structure is shown as a brown rectangular prism. The trees are rendered as green cones. The flame is visualised through isosurfaces of heat release rate per unit volume (>100 kW/m3). A sketch illustrating the view factor model is imposed on the drawing. The red line indicates a modelled rectangular flame and the black dashed lines indicate how much of the radiation from the flame arrives at the receiving surface on the structure.

exceed the predicted BAL, because as the fire width increases it is reasonable to assume the radiative heat flux on the structure will also increase.

Hilton et al. (2017) simulated the heat flux on an structure from a fire using SPARK. In their model the fire was modelled using the McArthur (1967) empirical model, and the radiative heat flux was calculated using a ray-tracing algorithm. The simulations of Hilton et al. (2017) did not attempt to replicate the scenarios specified in AS 3959, but instead simulated a fire moving past a structure.

The purpose of this study is to simulate a fire from an elevated fuel source like a shrubland and measure the radiative heat flux on a nearby house-like structure. In light of the results we offer some comments on the possibility of performance-based design using simulation results.

Numerical model

Physics-based fire simulation

Wildland-Urban Fire Dynamics Simulator (WFDS) is used to simulate burning of an idealised shrubland and measure the radiation heat flux received at a house-like structure. WFDS simulations of burning single trees have been carefully validated (Mell et al. 2009). Simulations of radiation heat load on structures from prescribed forest fires have been conducted by Hostikka et al. (2008). Hostikka et al. considered a prescribed fire, that is one where the intensity is prescribed a priori rather than computed by simulating pyrolysis and combustion reactions. Here we simulate a dynamic fire with full physics.

WFDS uses a large eddy simulation (LES) approach to modelling fluid momentum. That is, the largest turbulent eddies are resolved on the grid, and smaller turbulent motions are modelled using the default Deardoff sub-grid scale model (McGrattan et al. 2013b). Solid phase pyrolysis is modelled using the linear model of Morvan and Dupuy (2004). Gas-phase combustion is simulated using a mixture-fraction combustion model. For complete details see McGrattan et al. (2013a, 2013b).

Model setup

The shrubland is comprised of pine trees, 2.25 m tall on a surface of grass. While pine trees and grass surface fuel are an unusual choice to replicate Australian shrubland, validated fuel property measurements exist (Mell et al. 2007, Mell et al. 2009) and therefore we can be confident that simulating pine trees yields realistic results for pine shrublands. Note that, unlike Khan et al. (2019), a replication of AS 3959, as close as possible, is not attempted here. To replicate AS 3959 would require a study of the fuel types, such as the shrublands considered by Anderson et al. (2015), listed in the standard. Thermo-physical and chemical properties of the fuels would have to be measured and the simulations of combustion of shrubland samples would need to be validated against experiments.

The forested area is 37 m long and starts 45 m from the domain inlet. The trees are regularly spaced in a staggered fashion in four columns. The trees are spaced 2 m apart; alternating between columns of 16 and 17 trees. The tree is modelled as a cylindrical trunk and the crowns are modelled only as pine needles with 2.2 kg/m3 bulk density in a conical shape. The overall domain is 124 m long, 12 m wide, and 25 m tall. The domain size is chosen as the largest domain studied by Moinuddin and Sutherland (2019) and can accommodate a realistic house like structure. 200 mm grid resolution was used throughout the domain; the domain size and grid resolution were shown to be sufficient to ensure numerically converged heat release rate results (Moinuddin and Sutherland 2019) which are free of errors caused by under resolving the simulations. The inlet is a power law (1/7) model of the atmospheric boundary layer (ABL) with a wind speed of 3 m/s at 2 m. The two lateral edges use a symmetry boundary condition to force the fire to remain approximately straight throughout the simulation. Constant pressure boundary conditions are used at the top and outlet of the domain. The house is modelled as a solid, but thermally inert, obstruction located 25 m downstream of the shrubland. There is no combustible fuel between the shrubland and the house. The house structure is relatively small: 10 m long, 8 m wide, and 4.5 m tall. There is no attempt to reproduce detailed features of a house. The idea is that the centre of the front wall will receive most of the radiative heating and therefore the centre of the front wall is of the most interest. The rest of the house shape is then somewhat irrelevant to these simulations. A rendering of the domain showing the fire progression is shown in Figure 1.

Results and Discussion

Fire spread results

The location of the fire front as a function of time is computed from the centerline (y=0) heat release rate (HRR) data. The HRR data is first examined over all times to measure the maximum observed HRR. HRR data that are less than 1% of the maximum observed HRR are set to zero. The remaining nonzero HRR data are set to one. This filtering process effectively yields a black and white image of the flame based on the threshold of 99% of the maximum HRR. At each output time step, the geometric centroid of the flame image is computed, and the x-component of the centroid is taken as the flame front location. The flame centroid data is slightly noisy and depending on instantaneous flame geometry, the flame centroid can move backwards between observations.

Time is measured from the ignition time and the x-distance is measured as the distance from the ignition location.

The fire front location is plotted in Figure 2. Two distinct regions of propagation are observed; from time 0 to 20 s, the fire propagates along the surface, but at time 20 s the fire enters the crowns of the trees. The total fire intensity is plotted against time in Figure 3. A quasi-steady intensity is achieved at time 30 s. The intensity decreases at time 80 s as the fire reaches the end of the burnable region. The quasi-steady region is observed between 30 and 80 s.

The flame angle is computed from threshold HRR images. Following Cobian- Iñiguez et al. (2019) an ellipse is fitted to the HRR image at every time level. The ellipse is constrained so that the second moment of the ellipse is equal to the second moment of the nonzero region of the image. This process results in the ellipse that best overlaps the irregular flame shape. The length of the major axis of the ellipse and the orientation angle of the ellipse then corresponds to the flame length and flame angle respectively.

The flame angle is plotted in Figure 4. Initially, the flame is close to vertical. As the fire transitions from the surface to the crown at around time 20 s, the flame angle varies around an average of 62 degrees. Here, 90 degrees corresponds to a vertical flame, 0 degrees corresponds to a perfectly attached flame moving in the windward direction. Negative flame angles correspond to a flame that leans into the oncoming wind. There is no angle model within AS 3959, instead the flame angle is chosen to maximize the radiant heat flux on the structure, modelling the worst-case scenario. For a structure on flat ground the worst possible flame angle would be 90 degrees.

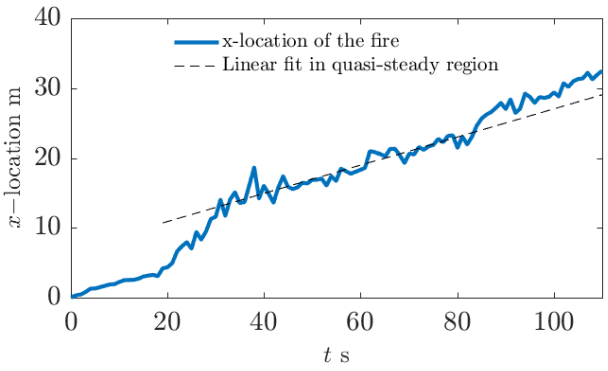

Figure 2: Fire front location as a function of time. A linear fit to determine the rate-of-spread after the crown fire developed is also shown. The rate-of-spread is 0.2 ms-1.

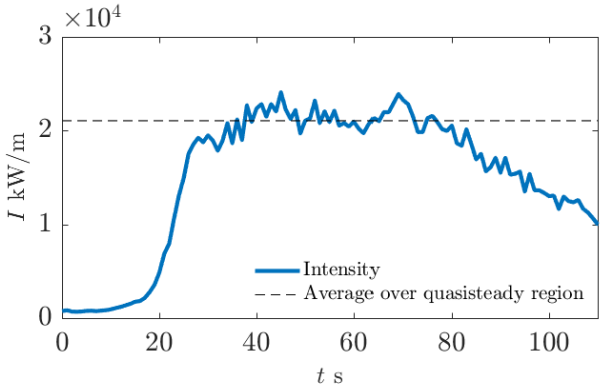

Figure 3: Fire line intensity as a function of time.

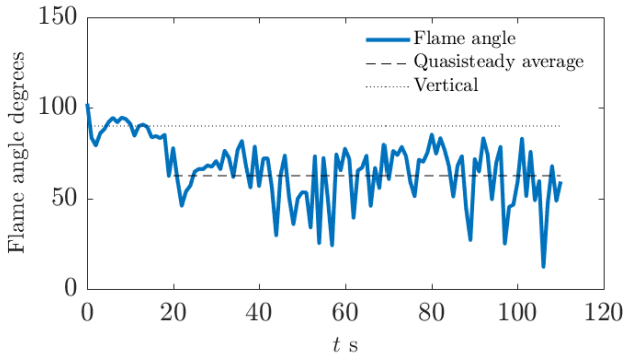

Figure 4: Flame angle in degrees as a function of time. The dotted line indicates a constant vertical flame, and the dashed line is the average flame angle in the quasi-steady region.

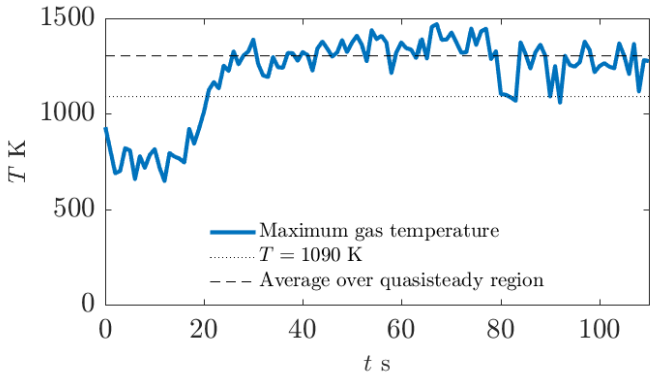

Figure 5: Maximum gas temperature as a function of time, compared to the AS 3959 assumption of 1090 K, and compared to the time-average maximum gas temperature over the quasi-steady region.

The maximum centerline gas temperature is taken as a proxy of the flame temperature. The mean flame temperature as a function of time is plotted in Figure 5. The flame temperature is found to be more than the 1090 K assumed in AS 3959 at approximately 1400 K; therefore, the radiant heat incident on the structure may be underestimated by AS 3959. Interestingly, even though the fire line intensity starts to decrease at around time 80 s, the maximum gas temperature remains approximately constant; probably because the maximum gas temperature related to the flame temperature and will largely be independent of the volume of over where the heat is released (ie. the intensity).

Heat flux at the structure

The radiative and convective heat fluxes at the structure are plotted in Figure 6 as a function of fire distance from the structure. The front face of the structure is set at $x = 0$ m and negative distance represents fire upstream of the structure. Both heat fluxes are very small, the maximum BAL level assumes 40 kW m -2. The maximum radiative heat flux received is 500 W m-2. The incident heat flux is likely insufficient to cause an ignition of a real structure. Note that there is a 25 m vegetation free zone before the house, and this distance is sufficient to ensure the radiant heat flux is small in this case. The radiant heat continues to grow as the fire approaches the structure. The magnitude of the radiant heat flux at the distances considered is of comparable size to the radiant heat flux simulated by Khan et al. (2019).

The distance between the flame and the structure is the crucial factor to consider when computing the expected heat fluxes on the structure. However, given the domain in these simulations is much narrower (12 m) than assumed by AS 3959 it is worth calculating the ratio of heat flux from the narrow and full width fires, using the AS 3959 model. Using the values and models prescribed for shrubland we find that for a 12 m wide fire, the predicted heat flux is approximately one third of the value predicted for the 100 m wide fire.

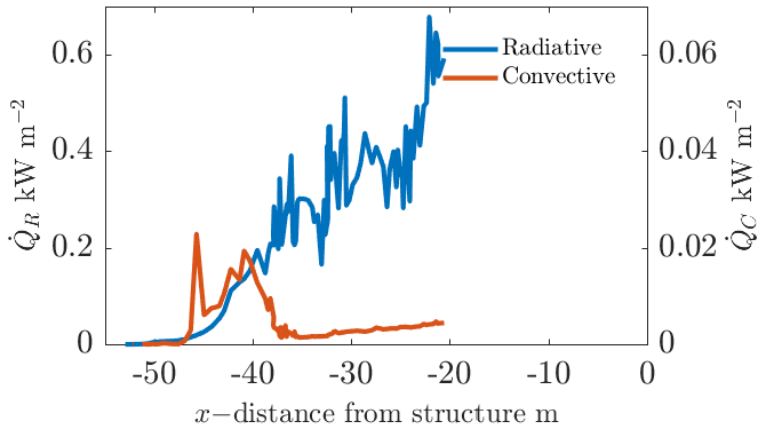

Figure 6: Radiative and convective heat fluxes received at the front face of the structure. Note that distance is measured from the centre of the fire to the front face of the structure. Negative distances represent a fire upstream of the structure. Note that the convective heat flux is shown on a scale an order of magnitude less than the scale of the radiative heat flux.

The convective heat flux on the structure is even smaller than the radiant heat flux. The flame angle is approximately 60 degrees throughout the simulation, and so the convective transport of heat will be predominantly vertical. When the flame angle is small the convective heat load is marginally higher but likely still negligible. This observation may appear at odds with Finney et al. (2015) who demonstrate that convective heat transfer is vital for the ignition of grass-like fuels. This is because the grass-like fuel is highly porous, has a large surface area, and is much closer to the flame. The plume temperature decreases rapidly away from the flame due to mixing of ambient air. The flow of the hot gasses over the house-like object is also considerably different to the flow through a porous fuel bed, resulting in a considerably lower convective heat flux on the surface of the structure.

Future work

Further work is required to model realistic Australian fuel types. Some measurements of Eucalyptus fuels have been made (Wadhwani et al. 2017) which would allow simulation of some of the fuel types specified in AS 3959. Those simulations could be used to verify or strengthen the BAL model within AS 3959.

Feasibility of performance-based design for bushfire prone areas

There is a possibility of performance-based design of structures in fire prone areas emerging as design tool in the near future. In this work, we have demonstrated that it is possible to simulate the impact of a design fire upon an idealised structure. Computational time constraints impede the simulation of larger fires on more realistic structures. Improvements to computational technology and development of refined physics based models will allow simulation of large scale fires on realistic houses. Therefore, performance-based design of structures must be considered. The simulated resilience of a structure to

fire impact can be optimized to meet certain prescribed criteria: eg the structure can withstand exposure to a wildfire for a sufficient period. Performance-based design would work on a case-by-case basis and if a structure satisfies the performance criteria, then the design is deemed suitable for construction. Two key points must be addressed before performance-based design of structures in a bushfire prone area can be adopted. (1) Design criteria, that is (at least) the intensity and duration of fire that a compliant building is expected withstand, must be determined. (2) Physics-based modelling of impact upon structures must be carefully validated against experimental or field observations to ensure that design scenarios are reasonably simulated. Importantly, firebrands must be incorporated into physics-based models. Firebrands were found to be the leading cause of house loss in the 2003 Canberra bushfires (Bianchi and Leonard, 2005). Significant advances in the simulation of ballistic firebrands (eg. Thurston et al. 2017, Wadhwani et al. 2019) have been made. However, none of these works consider the impact of firebrands on structures and none of these works consider ember showers and transport of embers that remain close to the ground.

While it seems possible that both of these points can be satisfactorily addressed, it will be some time before physics-based simulations of realistic fires impacting on proposed structures will become a routine part of the design process.

Conclusions

The radiative heat flux at the front face of a structure from a fire in a pine shrubland has been simulated using a physics-based model. In the quasi-steady spread region, the maximum flame temperature was found be approximately 1400 K, greater than the 1090 K used by the model in AS 3959. The

flame angle was found to be approximately 60 degrees, which is less than the vertical flame that would be assumed under AS 3959 for flat ground. The maximum incident heat flux on the structure is low: 500 W m-2 however, that is likely due to the distance between the structure and the fire.

Khan et al. (2019) reported similar results: at 25 m from the structure the heat fluxes were negligible and well below the 12.5 kW m-2 limits prescribed by AS 3959. However, as the fire approached and overran the structure the simulated radiant heat flux in Khan et al. was commensurate or greater than the values prescribed by AS 3959. We expect that if the structure adjoined the shrubland, the structure would receive a significantly larger heat flux, at least in order-of-magnitude agreement with AS 3959.

Finally, we appraised physics-based simulations for performance-based design for construction in a bushfire prone area. Ultimately, firebrand impact upon structures will need to be included in simulations. Fire and heat flux impacting on idealised structures is currently feasible, but more research is required before performance-based design becomes routine.

Acknowledgements

This research was undertaken with the assistance of resources and services from the National Computational Infrastructure (NCI), Australia.

References

Anderson, WR, Cruz, MG, Fernandes, PM, McCaw, L, Vega, JA, Bradstock, RA, Fogarty, L, Gould, J, McCarthy, G, Marsden-Smedley, JB and Matthews, S 2015, 'A generic, empirical-based model for predicting rate of fire spread in shrublands', *International Journal of Wildland Fire*, vol. 24, no. 4, pp. 443-460.

AS 3959 2009, *Construction of Buildings in Bush Fire Prone Areas (AS 3959) Technical report*, Standards Australia, Sydney, NSW.

Blanchi R & Leonard J 2005, *Investigation of Bushfire Attack Mechanisms Resulting in House Loss in the ACT Bushfire 2003*, Technical report, Bushfire Cooperative Research Centre (CRC) Report.

Cobian-Iñiguez J, Aminfar, AH, Weise, DR & Princeva, M 2019, 'On the Use of Semi-Empirical Flame Models for Spreading Chaparral Crown Fire', accepted, in press, *Frontiers in Mechanical Engineering*.

Finney, MA, Cohen, JD, Forthofer, JM, McAllister, SS, Gollner, MJ, Gorham, DJ, Saito, K, Akafuah, NK, Adam, BA & English, JD 2015, 'Role of buoyant flame dynamics in wildfire spread', proceedings of the *National Academy of Sciences*, vol. 112, no. 32, pp. 9833-9838.

Hilton, J, Leonard, J, Blanchi, R, Newnham, G, Opie, K, Rucinski, C & Swedosh, W 2017, 'Dynamic modelling of radiant heat from wildfires', in proceedings of the *22nd International Congress on Modelling and Simulation (MODSIM2017)*, Tasmania, Australia, pp. 3-8.

Hostikka, S, Mangs, J & Mikkola, E 2008, 'Comparison of Two and Three Dimensional Simulations of Fires at Wildland Urban Interface', *Fire Safety Science,* vol. 9, pp. 1353-1364.

Khan, N, Sutherland, D, Wadhwani, R & Moinuddin, K 2019, 'Physics-based simulation of heat load on structures for improving construction standards for bushfire prone areas', *Frontiers in Mechanical Engineering*, vol. 5, pp. 35.

McArthur, AG 1967, 'Fire behaviour in eucalypt forest. Commonwealth Department of National Development', *Forestry Timber Bureau*, Leaflet 107, Canberra, ACT.

Mell, W, Jenkins, MA, Gould, J & Cheney, P 2007, 'A physics-based approach to modelling grassland fires', *International Journal of Wildland Fire*, vol. 16, pp. 1–22.

Mell, W, Maranghides, A, McDermott, R & Manzello, SL 2009, 'Numerical simulation and experiments of burning Douglas fir trees', *Combustion and Flame*, vol. 156, pp. 2023-2041.

Moinuddin, KAM & Sutherland, D 2019, 'Modelling of tree fires and fires transitioning from the forest floor to the canopy with a physics-based model', *Mathematics and Computers in Simulation*.

Morvan D & Dupuy J 2004, 'Modeling the propagation of a wildfire through a Mediterranean shrub using a multiphase formulation', *Combustion and Flame,* vol. 138, pp. 199–210.

McGrattan, K, Hostikka, S and Floyd J 2013a, 'Fire dynamics simulator, user's guide', *NIST special publication*, vol. 1019.

McGrattan, K, Hostikka, S, Floyd, J, Baum, HR, Rehm, RG, Mell, W et al. 2013b, *Fire dynamics simulator (version 6), technical reference guide*, NIST special publication 1018.

Thurston, W, Kepert, JD, Tory, KJ & Fawcett, RJ 2017, 'The contribution of turbulent plume dynamics to long-range spotting', *International Journal of Wildland Fire*, vol. 26, no. 4, pp. 317-330.

Wadhwani, R, Sutherland, D, Moinuddin, KAM & Joseph, P 2017, 'Kinetics of pyrolysis of litter materials from pine and eucalyptus forests', *Journal of Thermal Analysis and Calorimetry*, vol. 130, no. 3, pp. 2035-2046.

Wadhwani, R, Sutherland, D & Moinuddin, K 2019, 'Simulated transport of short-range embers in an idealised bushfire', in proceedings for the *6th International Fire Behavior and Fuels Conference,* International Association of Wildland Fire.

Worden, H, Beer, R & Rinsland, CP 1997, 'Airborne infrared spectroscopy of 1994 western wildfires', *Journal of Geophysical Research: Atmospheres*, vol. 102, pp. 1287–1299.